Experimental Neurology 247 (2013) 45–58

Contents lists available at SciVerse ScienceDirect

Experimental Neurology

journal homepage: www.elsevier.com/locate/yexnr

Chronic intranasal deferoxamine ameliorates motor defects and pathology in the α-synuclein rAAV Parkinson's model

Fabia Febbraro *[,1], Kathrine J. Andersen, Vanesa Sanchez-Guajardo, Noemie Tentillier, Marina Romero-Ramos *

CNS Disease Modeling Group, Department of Biomedicine, Aarhus University, DK-8000 Aarhus C, Denmark

ARTICLE INFO

Article history:
Received 24 December 2012
Revised 10 March 2013
Accepted 14 March 2013
Available online 24 March 2013

Keywords:
Dopaminergic
Proteinase K
MHCII
Microglia
Recombinant adeno-associated viral vector
Iron
T cells

ABSTRACT

Parkinson's disease is characterized by neuronal death in the substantia nigra and the presence of intracellular inclusions of α-synuclein in the Lewy bodies. Several lines of data support a role for iron in Parkinson's disease: iron is present in Lewy bodies, iron accumulates in the dopaminergic neurons in the substantia nigra, and Parkinson's disease is correlated with polymorphisms of several genes implicated in iron metabolism. Furthermore, iron can compromise the solubility of α-synuclein through direct interaction and can induce neurotoxicity *in vitro*. Here, we investigate the possible neuroprotective effect of the iron chelator deferoxamine *in vivo* to elucidate whether iron chelation can provide meaningful therapy for Parkinson's disease. Hence, we used a Parkinson's disease animal model based on unilateral injection of a recombinant adeno-associated viral vector encoding α-synuclein in the rat midbrain. Rats were treated with a novel deferoxamine delivery approach: 6 mg of the compound was administered intranasally three times a week for 3 or 7 weeks. The behavior of the animals and histopathological changes in the brain were analyzed. Our data show that although intranasal administration of deferoxamine in rats did not protect them from dopaminergic cell death, it did decrease the number of the pathological α-synuclein formations at the terminal level. In addition, this treatment resulted in changes in the immune response and an overall partial improvement in motor behavior. Taken together, our data show that *in vivo* iron chelation can modulate α-synuclein-induced pathology in the central nervous system. Our data suggest that chronic administration of intranasal deferoxamine may be a valid approach to limiting the mishandling of α-synuclein in the central nervous system observed in Parkinson's disease and slowing disease progression.

© 2013 Elsevier Inc. All rights reserved.

Introduction

Parkinson's disease is mainly characterized by dopaminergic cell death in the substantia nigra (SN) and the presence of characteristic intracytoplasmatic inclusions, called Lewy bodies (LBs), in the surviving neurons (Marti et al., 2003). LBs are primarily composed of fibrillar aggregates of α-syn but also contain other molecules, such as iron (Castellani et al., 2000; Spillantini et al., 1997). In addition to being the main component of LBs, the role of α-syn in the disease is further supported by the fact that point mutations or multiplication of the gene results in familial PD (Ross et al., 2008; Thomas and Beal, 2007). Several groups have shown that, similar to α-syn, iron homeostasis is altered in PD, and both the protein and the metal accumulate in brains affected by PD or other synucleinopathies (Perry and Yong, 1986; Youdim et al., 1989; Zecca et al., 2004). The correlations between polymorphisms of different genes involved in iron homeostasis (Transferrin, Transferrin receptor, Frataxin, Lactoferrin and Haemo-chromatosis-related protein gene) and the incidence of sporadic cases of PD also support a role for this metal in the neurodegenerative process (Borie et al., 2002; Oakley et al., 2007). Indeed, several findings corroborate a role for iron in the progression of PD neurodegeneration (Double et al., 2000; Gerlach et al., 1994). Accordingly, overexpression of ferritin or the use of iron chelators results in neuroprotection in toxic PD models, although this has never been tested *in vivo* α-syn-based PD models (Kaur et al., 2003; Matarredona et al., 1997; Shachar et al., 2004; Xu et al., 2008, 2010).

Iron accumulation has recently been proposed as an early marker of PD, suggesting that changes in iron handling are pathogenic events that could play causative roles in the disorder (Martin et al., 2008). However, whether increases of iron in the SN are a casual factor or a consequence of the disease is still debated, especially because the mechanisms of iron's interference with brain homeostasis are not completely understood (Berg et al., 2001; Thompson et al., 2001). It has been shown *in vitro* that ferrous iron (Fe^{2+}) promotes oxidative stress (Beal, 1992; Gutteridge, 1992), which may contribute to the oxidative damage found in PD and might indirectly influence other

* Corresponding authors at: CNS Disease Modeling Group, Dept Biomedicine, Aarhus University Ole Worms Alle 3, bldg 1170, Aarhus C, DK-8000, Denmark. Fax: +45 86131160.
E-mail addresses: fabia.febbraro@ki.se (F. Febbraro), mrr@biokemi.au.dk (M. Romero-Ramos).
[1] Current address: Lab. of Molecular Neurobiology, Department of Medical Biochemistry and Biophysics, Karolinska Institute, Stockholm, Sweden.

0014-4886/$ – see front matter © 2013 Elsevier Inc. All rights reserved.
http://dx.doi.org/10.1016/j.expneurol.2013.03.017

proteins, such as α-syn. Further supporting this idea, *in vitro* studies have shown that iron can bind to α-syn and promote its aggregation by inducing α-syn oxidation (Cole et al., 2005; Golts et al., 2002; Gotz et al., 2004; Hashimoto et al., 1999). Additionally, recent data have revealed a possible direct link between the presence of iron and α-syn expression based on the existence of a putative iron responsive element in the 5′ untranslated region of human α-syn mRNA (Friedlich et al., 2007). Accordingly, we have shown *in vitro* that α-syn expression is modulated by iron at the translational level (Febbraro et al., 2012). Furthermore, it has recently been proposed that α-syn is a ferrireductase that can reduce Fe^{3+} to Fe^{2+} (Davies et al., 2011). Although a direct correlation between iron and α-syn in PD has not yet been fully proven, it is clear that both the protein and the metal are crucial for correct brain function.

Due to the role of iron in oxidative stress, iron chelators have been used as a neuroprotective strategy in different *in vitro* and *in vivo* neurotoxic models of PD. Deferoxamine (DFO), one such chelator, acts by binding Fe^{3+} and thereby preventing iron ions from catalyzing redox reactions that lead to free radical formation (Cullen et al., 2009). DFO was first used for the treatment of disorders related to iron overload and has been shown to protect neurons in the 6-OHDA and MPTP animal models of PD (Ben-Shachar et al., 1992; Kaur et al., 2003; Shachar et al., 2004). In the present study, we use a recently validated intranasal drug delivery approach to administer DFO more efficiently to the CNS (Hanson et al., 2009) in an animal model of PD based on the overexpression of α-syn using recombinant adeno-associated viral (rAAV) vectors. Our data show that although DFO treatment does not result in significant protection against nigral dopaminergic cell death in the α-syn overexpressing animals, it has an effect on the number of α-syn species that accumulate pathologically and the microglia response. These effects resulted in partial protection from the motor defects induced by α-syn overexpression. Taken together, our findings support a role for iron in α-syn-induced neuropathology and suggest that iron chelation may be meaningful in the treatment of PD.

Materials and methods

Recombinant adeno-associated viral vector production

The rAAV2/5 vector produced contained the coding sequence for the wild-type human α-syn under the control of a chimeric promoter consisting of an enhancer element from cytomegalovirus followed by the chicken β-actin promoter and flanked by AAV2 Inverted Terminal Repeats (Xu et al., 2001). The vector was produced by co-transfection of HEK293 cells with a pTR-UF20 plasmid containing the human α-syn gene with a helper plasmid containing the necessary adenoviral packing genes. The rAAV2/5 vector (rAAV2 vector packaged in AAV5 capside) was purified by iodixanol step gradients and ion-exchange chromatography as described previously (Zolotukhin et al., 1999, 2002), and vector titer was determined by quantitative PCR. The final titer for the vector was 8.0×10^{12} genome copies/ml.

Animals, surgery and intranasal drug delivery

Adult female Sprague Dawley rats (n = 64) from Taconic, Denmark, were used for the experiments. Animals weighed 225–250 g at the beginning of the experiment. They were housed three in a cage with *ad libitum* access to food and water and exposed to a 12 h light/dark cycle according to regulations of the Faculty of Health Sciences, Aarhus University, which adhere to Danish and EU law. All experimental protocols were previously approved by the Danish Animal Experiments Inspectorate.

For surgery, rats were anesthetized with a mix of dormitor-fentanyl (40 mg/kg body weight, i.p.). The surgical procedure was carried out using a stereotactic frame (Stoelting, Wood Dale, IL, USA). The rat scalp was incised along the midline to expose the bregma. Next injection coordinates for viral vector delivery were calculated. The coordinates were the following: anteroposterior −5.5 mm; lateral, −2.0 mm; ventral, −7.2 mm to dura, (nose −3.3). Two microliters of viral vector suspension were released unilaterally into the SN of the brain with a Hamilton syringe fitted with a glass capillary (outer diameter 60–80 μm) needle at the rate of 0.2 μl/30 s. The needle was left in position for an additional 5 min before being slowly retracted. Animals were then sutured with metal clips and, when fully awake, returned to their cage where food and water were freely available. For histological analysis, animals were sacrificed at 4 (n = 32, 16 in the DFO group and 16 in the control group) or 8 weeks (n = 32, 16 in the DFO group and 16 in the control group) from the time of injection.

Rats (n = 32, each group) were treated intranasally with either 10% DFO (6 mg per dose, Sigma) or saline solution (vehicle, for the control group) that was adjusted to a pH of 4.65. The solutions were administered as five doses of 12 μl solution (6 μl for each nostril) for a total volume of 60 μl. There was a 2 min gap between each of the five doses. The administration was performed in awake rats and required two persons; one person held the animal lightly with the nostrils exposed, and the second person placed the drops in the nostrils using a pipette. The rats were treated 3 times a week for a period of either 3 or 7 weeks starting one week post-surgery.

Behavioral analysis

Stepping test

During the 7th post-surgery week, animals were tested for forelimb akinesia using a stepping test that has been described previously (Olsson et al., 1995). On the two days prior to the test, the experimenter handled the animals to familiarize them with the test procedure. The test was performed two times per day for 3 consecutive days. The experimenter, blinded to the animal's treatment, held the animal, immobilized the hind limbs with one hand, immobilized the forepaw that was not tested with the other hand, and allowed the free forelimb to touch the table. The number of adjusting steps was counted while the rat was moved sideways along the table surface (90 cm in 5 s) in both forehand (*i.e.*, the animal was pulled to the left when the right paw was unrestrained) and backhand directions. As suggested in previous papers (Kirik et al., 1998), the backhand stepping scores were used as a control for animal performance, and the measurements of the forehand steps were used to evaluate motor impairment. The mean data obtained on the three days constituted the dependent variable.

Cylinder test

The cylinder test is a drug free test that is used to quantify forelimb use in animal models of PD (Schallert et al., 2000). The animals were tested at 4 and 8 weeks post-surgery after being placed in a 20 cm wide clear glass cylinder in which they could move freely. The experiment was videotaped. Mirrors were placed behind the cylinder to ensure all paw placements around the cylinder were visualized. An observer blinded to the animal's treatment viewed the videotapes and counted a minimum of 20 forelimb contacts with the cylinder wall. The number of contralateral (left) forelimb contacts, expressed as a percentage of total contacts, was the actual dependent variable.

Drug-induced rotation tests

Drug-induced rotation tests were assessed 8 weeks post-surgery in automated rotometer bowls after injection of D-amphetamine sulfate (2.5 mg/kg, i.p., Fagron, The Netherlands). Performance was monitored for 90 min. Data (net turns per minute) were analyzed by an experimenter blinded to the animal's treatment.

Histology

Perfusion and tissue processing

At 4 or 8 weeks post-surgery, animals from each group were deeply anesthetized with pentobarbital and perfused through the ascending

aorta with ice-cold isotonic saline, followed by 4% paraformaldehyde in 0.1 M phosphate buffer pH 7.4. Brains were removed and post-fixed for 2 h in the same solution and thereafter transferred to 20% sucrose in 0.1 M phosphate buffer before being sectioned on a freezing-stage microtome at 35 μm. The preceding steps were performed by an experimenter blinded to animal identity. In the coronal plane of the forebrain, 8 series were collected that extended from the prefrontal cortex to the end of the striatum to include the entire striatum (this yielded approximately 14 sections within striatum/series, each section in the series was separated by 8 × 35 μm = 280 μm). From the end of the striatum to the beginning of the cerebellum, 6 series were collected to include the full SN (this yielded approximately 9–10 sections/series within the SNc, and the sections of the series were separated by 6 × 35 μm = 210 μm).

Immunohistochemistry and histological staining

Immunohistochemical staining was carried out on free-floating sections using primary antibodies against tyrosine hydroxylase (TH, 1:3000, mouse monoclonal; Chemicon, Temecula, CA); VMAT2 (1:2000, rabbit polyclonal; Chemicon); human α-synuclein (1:4000, rabbit IgG polyclonal epitope 116-131); MHC II (1:250 mouse monoclonal; Serotec); CD68 (1:200 mouse monoclonal; Serotec); CD4 (1:500 mouse monoclonal; Serotec) and CD8 (1:500 mouse monoclonal; Serotec). The sections were rinsed three times in potassium-phosphate buffer (KPBS) between each incubation period. The sections were then quenched for 10 min in 3% H_2O_2 and 10% methanol in KPBS and pre-incubated for 1 h with 5% normal serum and 0.25% Triton X-100 in KPBS. The sections were incubated overnight at room temperature with primary antibody in 2.5% normal serum and 0.25% Triton X-100 in KPBS. This was followed by incubation with a 1:200 dilution of the appropriate biotinylated secondary antibody (Vector Laboratories, Burlingame, CA Vector Laboratories). Thereafter, sections were washed with KPBS, incubated with avidin–biotin–peroxidase complex (ABC Elite, Vector Laboratories, Burlingame, CA Vector Laboratories), and visualized using 3,3-diaminobenzidine (DAB) as a chromogen. Sections were mounted on chrome alum-coated slides, dehydrated in ascending alcohol concentrations, cleared in xylene and coverslipped in DePeX mounting medium.

For cresyl violet staining, the coverslip was removed from the sections in a xylene bath, and the samples were re-hydrated in descending alcohol concentrations. This step was followed by equilibrating the sections with an acetic acid solution before briefly staining them with 0.5% cresyl violet pH = 3.9. Sections were dehydrated in descending ethanol concentrations and cleared in xylene. The slides were coverslipped in DePeX mounting medium.

Perls staining was carried out on floating sections to detect ferric iron in brain. Sections were stained for 30 min in a mix of 2% potassium ferrocyanide and 2% HCl in KPBS. Thereafter, sections were quenched for 15 min with 10% methanol and 10% H_2O_2 in KPBS. Sections were washed in KPBS, incubated with avidin–biotin–peroxidase complex (ABC Elite) and visualized using DAB as a chromogen. Sections were then mounted on chrome alum-coated slides as described above.

Proteinase K digestion

Proteinase K treatment was performed on free-floating sections (Hoepken et al., 2004). Sections were first rinsed three times in KPBS and quenched for 10 min in 3% H_2O_2 and 10% methanol in KPBS. Thereafter, sections were rinsed in KPBS and heated in a water bath for 30 min at 80 °C. For PK treatment, sections were incubated with 5 mg/ml PK (Invitrogen) in KPBS for 20 min at room temperature. As a control, slices not treated with PK were incubated only in KPBS. Thereafter, sections were washed in KPBS three times, mounted on chrome alum-coated slides and dried overnight. Immunohistochemical staining was performed on the mounted sections using primary antibody against pan-synuclein (1:1000 rabbit IgG polyclonal; Abcam ab6176) in 2.5% normal serum 0.25% Triton X-100 in KPBS. This was followed by incubation with a 1:200 dilution of biotinylated anti-rabbit IgG antibody. Sections were washed with KPBS, incubated with avidin–biotin–peroxidase complex (ABC Elite), and visualized with DAB as a chromogen. Thereafter, sections were dehydrated in ascending alcohol concentrations, cleared in xylene and coverslipped in DePeX mounting medium. For semi-quantification, 3 representative 10× photos per striatal section were taken, and α-syn+ aggregates were counted by a researcher blind to the identity of the section. The numbers of aggregates per photo were averaged for each animal and later for each group.

Stereological quantification of cells

Estimation of the total number of TH-positive (TH+) cells in SN was made with unbiased stereology using the optical fractionator as previously described (Kirik et al., 2002). This sampling technique is not affected by tissue volume changes and does not require reference volume determinations (West, 1999). Sampling was performed using the NewCAST software from Visiopharm. A low power objective lens (1.25×, SPlan) was used to delineate the borders of the SN at all levels in the rostro-caudal axis. The medial border of the SN was defined by a vertical line passing through the medial tip of the cerebral peduncle (and by the medial terminal nucleus of the accessory nucleus of the optic tract, when it was present in the sections); thereby, TH+ cells in the ventral tegmental area (VTA) were excluded. The ventral border followed the dorsal border of the cerebral peduncle; thereby TH+ cells in pars reticulata (SNr), the area extending laterally to include the pars lateralis, and pars compacta SNc were included. The sections used for counting covered the entire SN from the rostral tip of the SNc back to the caudal end of the SNr. This typically yielded 9–10 sections in a series. The counting was performed in a blind manner. The counting frame was placed randomly on the first counting area and systematically moved through all counting areas until the entire delineated region was sampled. The sampling frequency was chosen by adjusting the X–Y step length between 150 and 200 μm such that approximately 100–200 TH+ cells were counted in each side of the SN. Actual counting was performed using a 40× objective (NA 0.75). The estimates of the total numbers of neurons were calculated according to the optical fractionator formula, and a coefficient of error <0.10 was accepted (Gundersen and Jensen, 1987; West, 1999). The same procedure was used to count VMAT2+ cells in randomly chosen animals.

Estimation of the total number of MHCII+ microglia in the striatum was preformed similarly. A low power objective lens (1.25×, SPlan) was used to delineate the borders of the striatum at all levels in the rostro-caudal axis while excluding the most caudal part of striatum where the hippocampus was visible; this typically yielded 11 sections for counting. Counting was performed in a blind manner, and the sampling frequency was chosen by adjusting the X–Y step length between 100 and 200 μm. Actual counting was performed using a 40× objective (NA 0.75). The estimates of the total numbers of cells were calculated according to the optical fractionator formula, and only animals with a coefficient of error <0.1 after counting were included in further analyses (Gundersen and Jensen, 1987; West, 1999).

Striatal fiber density measurement

The optical density of TH+ fibers in the striatum was measured for each animal by densitometry at 6 different rostro-caudal levels according to the rat brain atlas (Paxinos and Watson, 2007) (1.6; 1.00; 0.20; −0.30; −0.92; −1.40 mm from Bregma). The slides were scanned in a densitometer (BioRad GS-710) and analyzed for gray intensity using the ImageJ 1.42 program. Data are presented as a percentage of the intact control side. Calibration of the program was performed with a "calibrated optical density step tablet" to obtain optical density values according to the instructions on the program's web page (http://rsb.info.nih.gov/ij/docs/examples/calibration/index.html). To estimate the specific TH staining density, the optical density readings were corrected for

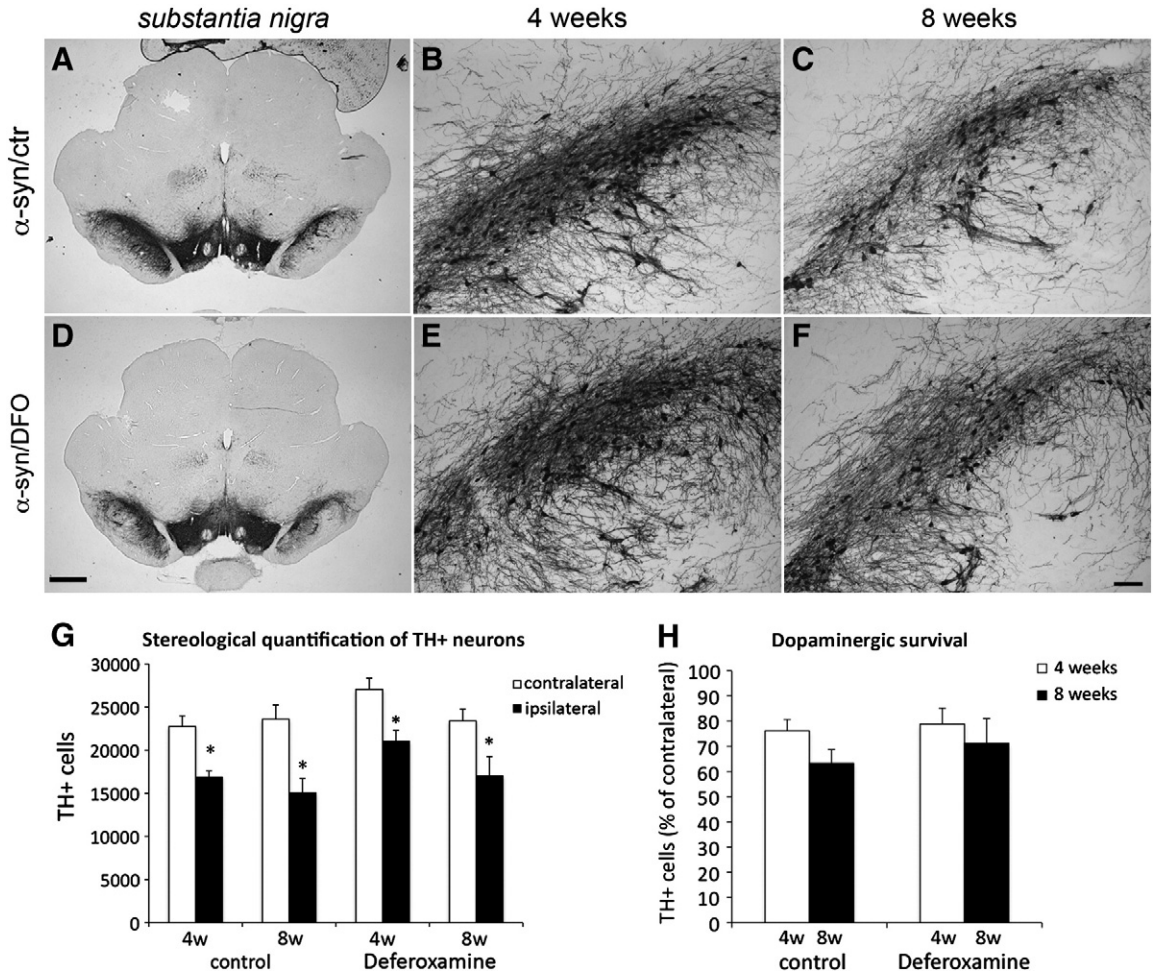

Fig. 1. TH immunohistochemical staining of nigral sections. Animals injected with rAAV5-α-syn (A–F) vectors and treated with ctr (A–C) or DFO (D–F) at 4 weeks (B, E), or 8 weeks (A, D, C and F). In panels C and F, higher magnification pictures of the right SN from sections shown in panels A and D, respectively, are presented. (G) Bar graph showing the stereological estimation of TH + cell in the contralateral and ipsilateral SN (average ± SEM). All groups at all time points showed a significant decrease in the TH + cells in the ipsilateral compared to the contralateral side. Paired *T*-test, $^{*}p < 0.05$, different from the respective contralateral side. (H) Bar graph illustrating dopaminergic survival: numbers of TH+ cells as percentages of the contralateral side (average ± SEM) in the α-syn/DFO and α-syn/ctr groups at two time points. The scale bar in F is 100 μm and applies to B; C; E; the scale bar in D is 1 mm and applies to A and D. α-syn, alpha-synuclein; ctr, control; DFO, deferoxamine; SN, substantia nigra; TH, tyrosine hydroxylase.

nonspecific background density by measuring the corpus callosum above each striatum. The data are presented as percentages of the intact side (contralateral striatum).

Analysis of α-synuclein accumulation in the striatum

To quantify the α-syn-positive (α-syn+) aggregations for each animal, four serial coronal sections (1.2 mm, 0.70 mm, −0.26 mm, and −0.80 mm from bregma) were immunostained with anti-human α-syn. One 20× photo (594 μm × 445 μm) per section was taken at the dorso-lateral level of the ipsilateral striatum; this area is rather spared in this model and therefore likely to contain high levels of α-syn (total 4 photos per animal). The photos were adjusted to increase contrast of the fibers immunostained for α-syn. A similar approach was taken for VMAT2 immunostained sections. Each photo was then analyzed with the ImageJ 1.42i program after setting a length scale and a threshold; thereafter, we obtained the numbers and areas (μm^2) of particles (circularity 0.3-1).

Microscope analysis for immune cells in brain sections

An observer blind to the identity of the samples analyzed 4–5 serial coronal sections from the striatum (distance 840 μm) and 3–4 sections from the SN (distance 630 μm) of each animal for each antibody tested. The sections used for analysis were obtained by sampling the entire striatum from the point where the corpus callosum crossed hemispheres (+1.6 mm from bregma) to the rostral part where the lateral globus pallidus and early hippocampus are observed (−1.8 mm from bregma). The midbrain sampling covered the SN from the rostral tip of the SNc (−4.6 mm from bregma) back to the caudal end of the SNr (−6.5 mm from bregma).

Analyses for MHC II and CD68 in the SN were performed at 10× and 40×, and the extent of the marking was scored as described in (Sanchez-Guajardo et al., 2010). The levels of CD68 expression were scored from 0 to 4 based on the number of CD68+ cells at that location. A score of 0 indicated no or few isolated positive cells; a score of 1 indicated few scattered cells; a score 2 indicted the presence of cells throughout the SNc; a score of 3 indicated the presence of cells throughout the SN; and a score of 4 indicated the SN was saturated throughout with CD68+ cells. The level of MHC II expression in microglia was scored on the following scale from 0 to 5: score 0, no positive cells; score 1, a few isolated cells; score 2, cells scattered throughout the SNc or in a few clusters; score 3, cells throughout the SNc; score 4, cells throughout the SN; and score 5, the SN was saturated with cells.

For CD4 in the SN, a series of coronal sections, similar to the series used for TH stereology, were used to count all CD4+ cells in each nigral section (typically 9 sections per series); the total and average numbers of positive cells counted per section were calculated for each

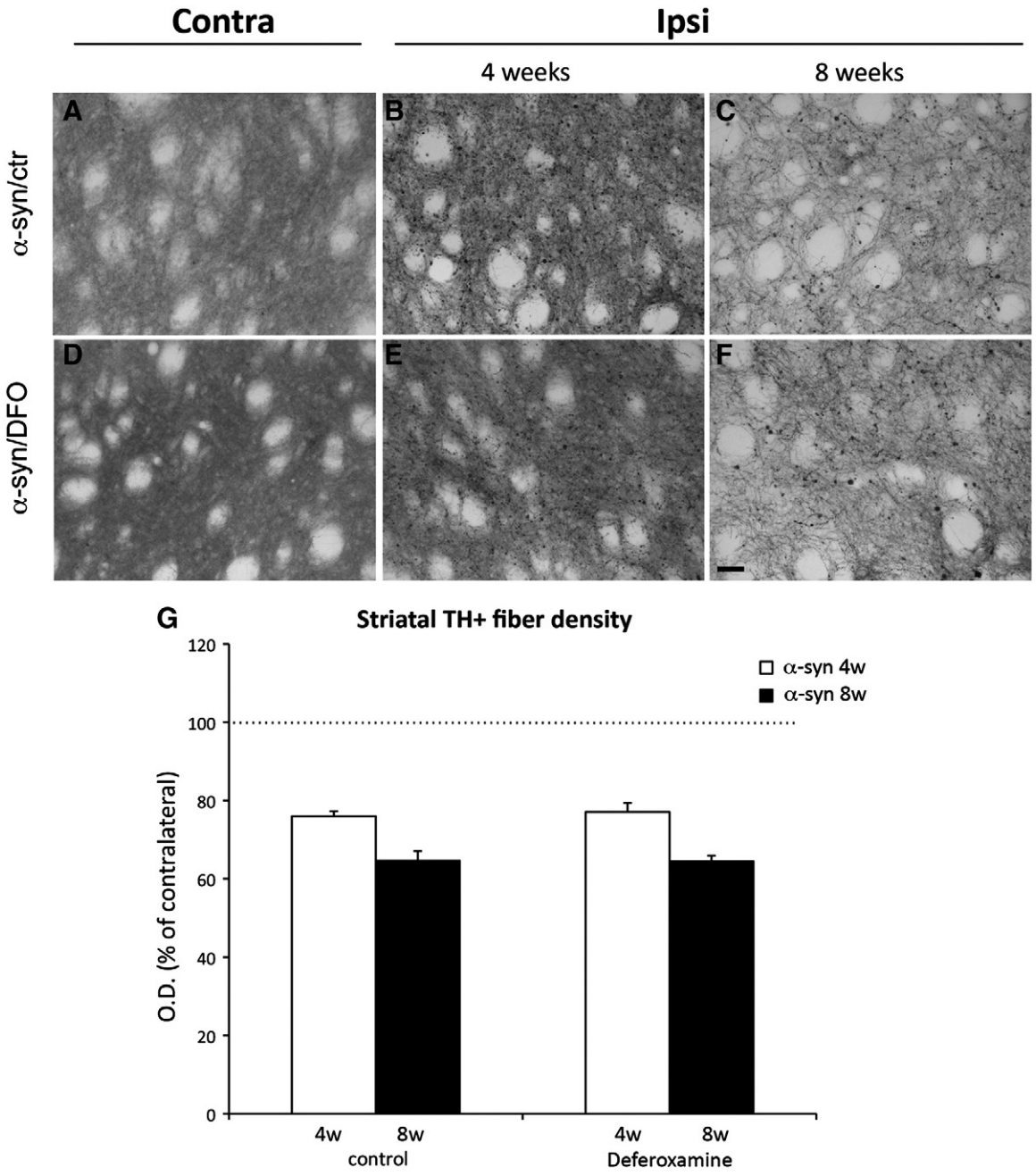

Fig. 2. Photomicrographs illustrating TH + fiber staining in the striatum. Animals injected with rAAV5-α-syn and treated with ctr, (A–C), or DFO (D–F) at 4 weeks (A, B–D, E), and 8 weeks (C, F). Panels A and D show the contralateral striatum of the section shown in panels B and E, respectively. As early as 4 weeks, abnormal thickening of TH + fibers was observed at striatal levels in both groups (B and E). At 8 weeks, significant loss of dopaminergic terminals was apparent in both groups (C and F). No obvious pathology or fiber loss was observed in the contralateral side (A and D). (G) Bar graph illustrating the semi-quantitative TH + densitometry measurements expressed as percentages of the intact side (average ± SEM). For each animal, 6 different rostro-caudal levels of the striatum were analyzed and later averaged. The scale bar in F is 50 μm and applies to all panels. α-syn, alpha-synuclein; DFO, deferoxamine; crt, control; TH, tyrosine hydroxylase.

animal, each group and each time. In the striatum, the observer counted the number of positive cells in one representative section. For CD8 only, one nigral and one striatal section were analyzed; the observer counted the number of positive cells within the section at 20× and 40×.

In all the experiments mentioned above, the experimenter was blind to the rats' identities.

Statistical analysis

Statistical comparison of data was performed using the JMP statistical software v. 5.01 (SAS Institute Inc. Cary, NC, USA). Time and group interactions were always first analyzed using a two-way factorial ANOVA. When appropriate, group or time effects were addressed separately using a one-way ANOVA. When needed, non-parametric Kruskal–Wallis tests were applied. Significance was accepted at the ≥95% probability level.

Results

α-Synuclein overexpression induced loss of dopaminergic neurons despite iron chelation

To elucidate the role of iron in α-syn-induced neurodegeneration, we used the iron chelator DFO in the rAAV-based PD model. It was

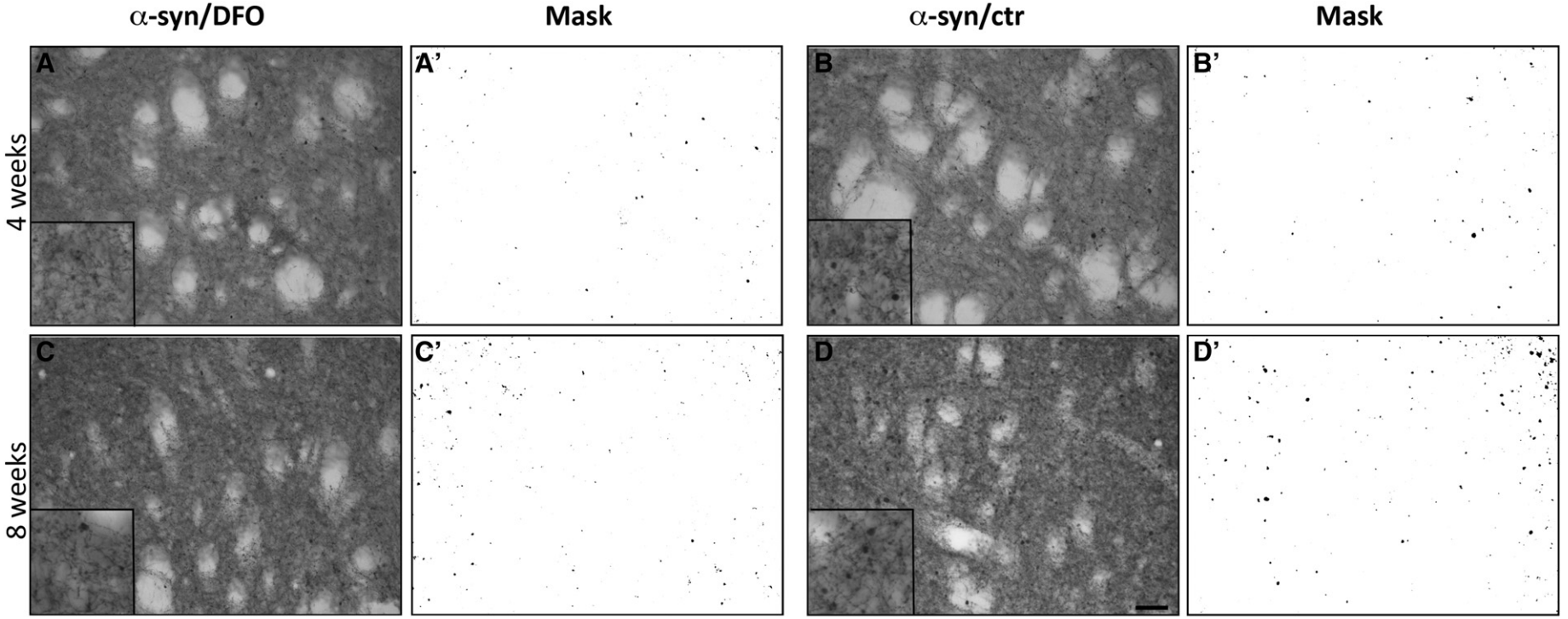
α-syn/DFO
Mask
α-syn/ctr
Mask
A
A'
B
B'
C
C'
D
D'
4 weeks
8 weeks

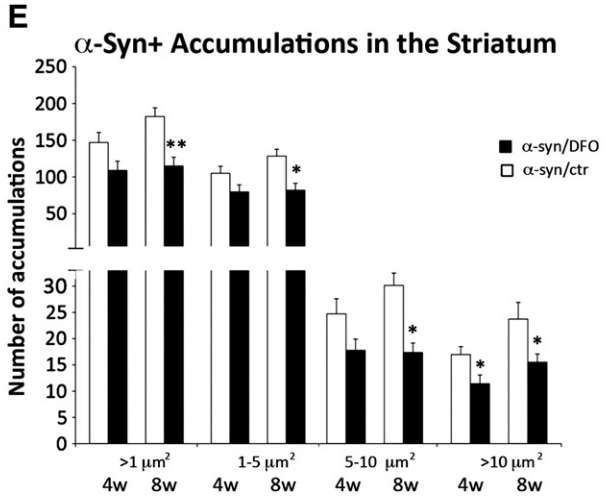
E
α-Syn+ Accumulations in the Striatum
Number of accumulations
α-syn/DFO
α-syn/ctr
>1 μm²
1-5 μm²
5-10 μm²
>10 μm²
4w
8w

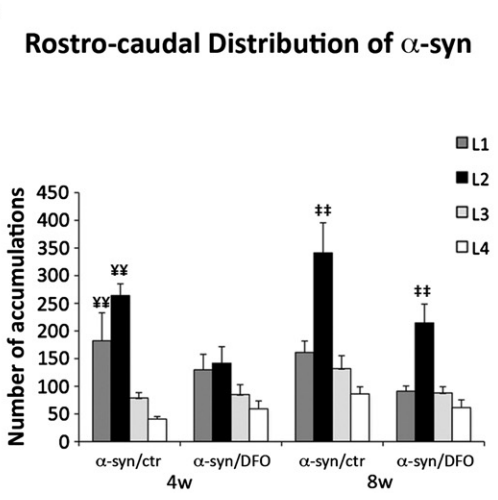
F
Rostro-caudal Distribution of α-syn
Number of accumulations
L1
L2
L3
L4
α-syn/ctr
α-syn/DFO
4w
8w

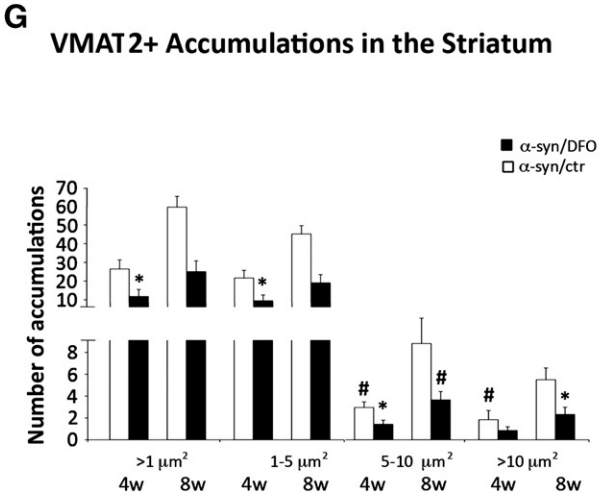
G
VMAT2+ Accumulations in the Striatum
Number of accumulations
α-syn/DFO
α-syn/ctr
>1 μm²
1-5 μm²
5-10 μm²
>10 μm²
4w
8w

recently shown that DFO efficiently reaches brain areas such as the striatum and midbrain when administered intranasally to rats and decreases the possible peripheral effects compared to intravenous injections (Hanson et al., 2009). Here, we used this approach in the rat α-syn model for PD; however, in contrast to the previous study, we administered DFO to wake animals. To avoid possible differences due to treatment related stress, a vehicle solution was applied to a control group. rAAV2/5 encoding α-syn was locally injected into the SN. The animals were subsequently treated 3 times a week with either 6 mg DFO (α-syn/DFO) or with a vehicle solution (α-syn/ctr) starting one week post-surgery and continuing to the 7th week.

α-Syn-induced dopaminergic toxicity was examined with TH staining at the nigral and striatal level. Analysis of TH immunostaining in the SN showed decreases of TH+ neurons in the side overexpressing α-syn when compared to the contralateral, uninjected side at all time points; this was true in both ctr and DFO α-syn-overexpressing animals (Figs. 1A–F). Stereological quantification of TH+ neurons in the SN showed that α-syn overexpression indeed induced significant losses of nigral TH+ neurons irrespective of the presence or absence of the chelator (Fig. 1G). The percentage of neuronal loss in the ipsilateral side compared to the contralateral uninjected side was 23.86% ± 4.5 for ctr, and 21.17% ± 6.3 for DFO after 4 weeks and 36.76% ± 5.45 for ctr and 28.81% ± 9.80 for DFO after 8 weeks (Fig. 1H). To confirm that this loss of TH+ neurons was due to cell death and not to down-regulation of the protein, we performed stereological analysis using VMAT2, which is an accepted alternative marker for dopaminergic neurons (Georgievska et al., 2004). Brain sections of randomly selected animals within each group were stained with anti-VMAT2, stereological quantification of SN neurons was performed, and results similar to those observed with TH were obtained (data not shown).

Inspection of TH-stained sections at the striatal level showed dense innervations throughout the striatum in the non-injected side in all groups (Figs. 2A and D). Analysis of the ipsilateral side revealed a time-dependent reduction of striatal TH+ fibers in the injected side irrespective of treatment (Figs. 2B–C and E–F). When analyzed by densitometry, the terminals were decreased to a similar extent in the α-syn overexpressing side after 4 or 8 weeks (Fig. 2G).

Iron chelation reduced and halted the formation of pathological α-synuclein accumulation in striatal fibers

Immunostaining of the SN with an antibody for human α-syn revealed numerous cell bodies expressing the transgene in the ipsilateral side after only 4 weeks; this number decreased after 8 weeks, most likely as consequence of the cell loss (Suppl. Fig. 1). All α-syn+ cellular profiles observed in the SN were fusiform as resembled neuronal-like cell bodies. As previously described, no glia-like cell bodies expressed the transgene (Burger et al., 2004). At the striatal level, α-syn overexpression resulted in α-syn+ fibers with discrete α-syn+ accumulations and thickening of fibers resembling dystrophic neurites (Figs. 3A–D). The α-syn+ striatal fiber staining decreased with time in both DFO and ctr groups, while the accumulations increased in size.

To address the changes induced by iron chelation in the α-syn terminals' pathological formations, we quantified the number of α-syn+ accumulations >1 μm^2 in striatum. We did so at 4 different rostrocaudal levels in the coronal striatal sections. In all sections, one photo of the lateral side of the striatum was taken (the area where fiber loss is less acute in this model; Suppl. Fig. 1 black arrow). Consistently, the rostral levels showed more aggregates than the caudal levels, and the second level (0.7 mm from bregma) always had the greatest number of aggregates (Fig. 3F). When the numbers of aggregates in all 4 levels were averaged to get a single number per animal, the DFO animals showed a trend toward fewer α-syn+ accumulations after 4 weeks ($F_{1,13} = 4.16$ $p = 0.06$) in striatum compared to ctr animals (Figs. 3A–E). Indeed at this time point, ctr animals also showed a significantly greater number of the most rare large α-syn aggregates (>10 μm^2) ($F_{1,13} = 6.0$ $p = 0.029$). At 8 weeks post-surgery, ctr animals showed significantly more α-syn+ accumulations of all sizes than the DFO treated animals (Fig. 3E). The ctr animals showed a slight increase in all aggregates of all sizes over time (Fig. 3E), while the DFO animals only showed a small increase in the number of large accumulations. This suggests that chronic DFO administration reduced the formation of α-syn pathological accumulations without preventing increases in their size.

We and others have previously observed that the pathological formations at the axonal level are also revealed upon immunohistochemistry with antibodies against VMAT2 and TH, suggesting the presence of these proteins in the accumulations containing α-syn. Accordingly, analysis of VMAT2+ pathological accumulations in the striatum showed that α-syn overexpression led to the presence of VMAT2+ formations >1 μm^2 that were significantly decreased by DFO treatment at 4 weeks ($F_{1,13} = 5.73$ $p = 0.03$) and 8 weeks ($F_{1,15} = 4.48$ $p = 0.05$) (Fig. 3G). In contrast to the α-syn+ accumulations, the VMAT2+ accumulations doubled in number after 8 weeks in both groups (Figs. 3E and G). Interestingly, when comparing the ratio α-syn/VMAT2+ accumulations at 4 weeks, ctr animals showed a ratio of 6 ± 0.8, while the ratio for the DFO group was significantly higher, 12 ± .2.5 ($F_{1,13} = 5.69$ $p = 0.03$). After 8 weeks, although the ratio remained unchanged in the ctr group (5.5 ± 0.9), the DFO animals showed a marked decrease in the α-syn/VMAT2+ accumulation ratio. This ratio reached a value similar to that of the control group at this time point (4.8 ± 1.0). These data suggest the following. First, not all α-syn+ accumulations possess VMAT2; therefore, the VMAT2 might be incorporated later. Second, DFO decreases the number of early VMAT2+ accumulations, but does not halt the incorporation of VMAT2 to α-syn+ formations as time progresses.

Fibrillar forms of α-syn are resistant to digestion by PK, an enzyme that exhibits strong proteolytic activity on denaturated and native proteins (Conway et al., 2000; Ebeling et al., 1974; Giasson et al., 2001; Miake et al., 2002). To explore whether the nature of α-syn+ aggregates was different between the DFO and the ctr groups, α-syn immunohistochemistry against rat/human α-syn levels was performed at 4 weeks at the striatal and hippocampal levels with or without PK pre-treatment. At the level of the hippocampus, PK treatment led to the disappearance of the endogenous α-syn+ signal in both groups (Figs. 4A–B and E–F). However, at the striatal level, although PK digestion

Fig. 3. Transgene expression in the dorso-lateral portion of the striatum. Animals injected with rAAV5-α-syn treated with DFO (A, C), or with ctr (B, D) at 4 weeks (A, B) or 8 weeks post-surgery (C, D). The inset in each photo shows a higher magnification detailing the pathological α-syn+ fibers. Panels A′, B′, C′, and D′, represent masks of the low magnification pictures in A, B, C, and D, respectively, created with the ImageJ 1.42 program. A robust transgene expression in fibers was detectable at all time points in all groups (A–D). (E) Bar graph illustrating the total numbers of α-syn+ accumulations >1 μm^2 and their size distribution in the lateral striatum in the ctr and α-syn/DFO groups at both time points (see Materials and methods section for a detailed description). At 4 weeks, DFO treatment reduced the number of large-size α-syn+ accumulations >10 μm^2 when compared to the control group (D and E). At a later time point, the α-syn accumulations in all the size range were significantly decreased in the α-syn/DFO group compared to ctr group (E). (F) Bar graph illustrating the numbers of α-syn+ accumulations >1 μm^2 at the four rostra-caudal levels examined in the striatum (see Materials and methods section for detailed description). Notice that higher numbers are observed in the more rostral levels, especially level 2 (0.70 mm from the Bregma). (G) Bar graph illustrating the numbers of VMAT2+ accumulations >1 μm^2 and their size distribution in the lateral striatum in the two groups at the different time points. At 4 weeks, DFO decrease the presence of VMAT2+ accumulations of small and medium sizes, while at 8 weeks DFO treatment resulted in fewer large accumulations compared to the control. All numbers are the average ± the SEM. No time × drug interaction was found, one-way ANOVAs of drug or time effect were used. *p < 0.05 and **p < 0.01 different from the other group at the same time point; #p < 0.05 different from the same group at the later time point. ¥¥p < 0.01 different to levels 3 and 4 in the same group; ‡‡p < 0.01 different from all other levels in the same group. The scale bar in D is 50 μm and applies to all low magnification photos, the scale bar is 20 μm for high magnification insets. α-syn, alpha-synuclein; DFO, deferoxamine; ctr, control.

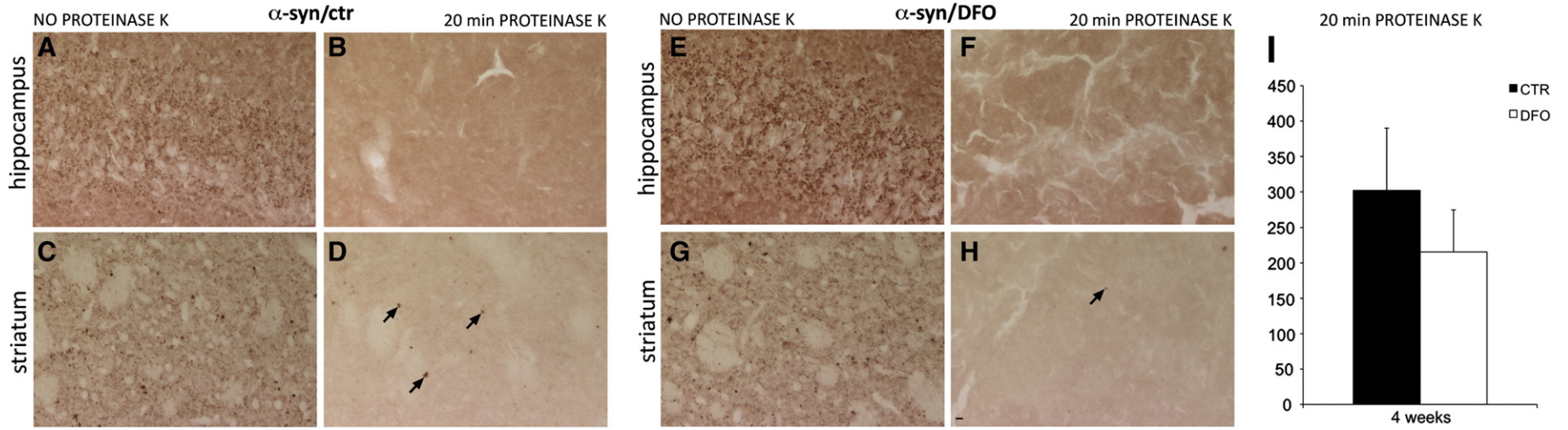

Fig. 4. The effect of proteinase K treatment on the striatum and hippocampus at 4 weeks. Human and rat α-syn expression in the hippocampus (A, B, E, F) and in the lateral striatum (C, D, G, H) of animals injected with rAAV5-α-syn treated with ctr (A–D), or with DFO (E–H) at 4 weeks after transduction. Sections were treated with 5 mg/ml PK in KBPS for 20 min (panel B, D, F, H) or with KPBS alone as control (panel A, C, E, G). The hippocampus showed an endogenous α-syn+ signal (A and E) that disappeared after PK treatment in both the DFO and ctr groups (B and F). At 4 weeks, numerous α-syn+ aggregates were observed in the striatum in both α-syn/ctr and α-syn/DFO animals (C and G). Upon PK treatment, PK-resistant α-syn+ aggregates (arrows) were more numerous in the α-syn/ctr group (D) than in the α-syn/DFO group (H). The number of α-syn+ aggregates (average ± SEM) was calculated in the striatal sections (see Materials and methods); although this number was lower in DFO animals, this difference did not reach significance (I). The scale in H is 16 μm and applies to all panels. α-syn, alpha-synuclein; DFO, deferoxamine; ctr, control; PK, proteinase K.

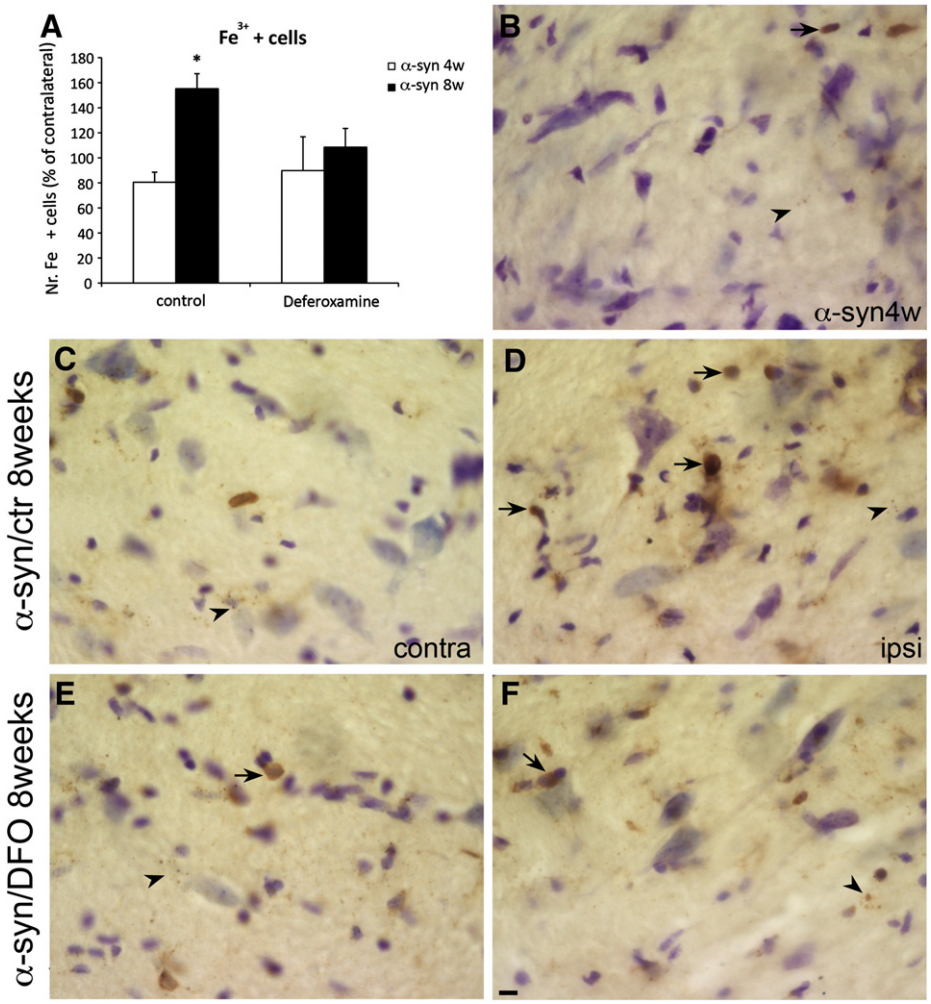

Fig. 5. Analysis and photos of Fe^{3+} containing cells in the SN. (A) Bar graph illustrating the numbers of Fe^{3+} positive cells per section expressed as percentage of the intact side (average ± SEM). The selective ipsilateral increase in Fe^{3+}-positive cells induced by α-syn overexpression was abolished by DFO treatment. Photomicrographs illustrating Fe^{3+}-positive cells in the SN in animals injected with rAAV5-α-syn, treated with ctr, (C–D), or DFO (E and F) at 8 weeks from transduction by a Perls staining and counterstained with cresyl violet. Panels C and E show the contralateral side of the sections shown in panel D and F, respectively. Panel B shows Fe^{3+}-positive cells in the ipsilateral side of the SN at 4 weeks from transduction. Two distinctive forms of staining were observed upon Perls staining: cells containing Fe^{3+} (black arrows in all panels) and discrete Fe^{3+}-positive accumulations not associated with cell bodies (arrowheads in all panels). Statistical analysis: non-parametric Kruskal–Wallis * $p < 0.05$ compared to the same group at earlier time point. The scale bar in F is 10 μm and applies to all panels. ANOVA, analysis of variance; α-syn, alpha-synuclein; DFO, deferoxamine; ctr, control; contra, contralateral; ipsi, ipsilateral; SN: substantia nigra.

resulted in a drastic reduction in the number of α-syn + accumulations in the ipsilateral side, we also observed the presence of resistant α-syn+ aggregates in both the DFO and, more obviously, in the ctr group (Figs. 4D and H). When semi-quantified, there was no significant difference in the number of striatal PK resistant aggregates between these two groups.

α-Synuclein overexpression induced an increase in Fe^{3+} containing cells that was attenuated by iron chelation

To establish the cellular presence of Fe^{3+}, Perls staining was performed, and the number of Fe^{3+} containing cells in the SN (both SNc and SNr) was counted (Fig. 5A). No difference in the number of Fe^{3+} containing cells between the ipsi- (cell number average ±SEM ctr 77 ± 18; DFO 80 ± 20) and contralateral sides (ctr 93 ± 17; DFO 81 ± 15) was observed at 4 weeks irrespective of treatment (Fig. 5A), and a bilateral increase in Fe^{3+} cells was observed with time in both α-syn groups (Figs. 5B–F). When comparing the ipsi- *vs.* contralateral sides at 8 weeks, ctr animals showed a greater number of cells containing Fe^{3+} in the injected side (233 ± 31) than in the control side (171 ± 32) ($F_{3,27} = 3.24$ $p = 0.039$) (Figs. 5A, D *vs.* C). However, chronic iron chelation prevented this differential increase of Fe^{3+} containing cells (192 ± 23 ipsilateral *vs.* 201 ± 36 contralateral) (Figs. 5A, F *vs.* E).

α-Synuclein overexpression induced nigral microglia activation

We have previously shown that α-syn overexpression induces changes in the microglia population that are related to the level of α-syn-induced pathology (Sanchez-Guajardo et al., 2010). Based on our own previous data, α-syn overexpression that results in cell death leads to an increase in CD68 expression in the SN (Sanchez-Guajardo et al., 2010). Accordingly, here microglia showed a robust increase in CD68 expression in the SNc of ctr animals from 4 weeks (Table 1). Iron chelation did not prevent this activation, in accordance with the presence of dopaminergic cell death in this group.

α-Syn overexpression led to a transient significant increase of MHC II+ microglia in the SNc of ctr animals at 4 weeks (Table 1; chi-square = 11.55 $p = 0.0007$). The presence of iron chelation did not fully prevent the increase in MHC II+ microglia in the SN, although this increase observed was less consistently in this group and was not significantly different than the DFO group's median at 8 weeks (chi square = 2.67 $p = 0.10$). As expected, no or very low

Table 1
Analysis of expression levels of microglia activation markers induced by overexpression of α-synuclein in the substantia nigra.

	4 weeks	8 weeks
CD68 substantia nigra		
α-syn/ctr	3.0 ± 0.5	1.0 ± 0.5 **
α-syn/DFO	3.5 ± 2.2	1.0 ± 1.7 *
MHC II substantia nigra		
α-syn/ctr	4.0 ± 1.0	2.5 ± 1.0 **
α-syn/DFO	4.0 ± 2.3	2.0 ± 2.6

Presence of CD68 and MHC II+ cells throughout the SN of animals treated with DFO (α-syn/DFO) or with vehicle (α-syn/ctr). An observer blind to the samples' identities scored expression levels from 0 to 4 for CD68 and 0 to 5 for MHC II based on the number of positive cells and area covered, as explained in the Materials and methods section. The median per animal was calculated followed by the group median. Numbers are group medians ± I.Q.R. Statistical analysis: non-parametric Kruskal–Wallis * $p < 0.05$ **$p < 0.01$ compared to the same group at earlier time point.

expression of the complex was detectable in the contralateral SN in all groups at both time points (not shown).

Iron chelation tended to decrease α-synuclein-induced antigen presenting microglia in the striatum

To analyze the microglia response in areas distant from the injection site where α-syn overexpression and pathology are relevant, we stereologically quantified MHC II+ cells in striatal sections. As expected, no or very low expression of the complex was detectable across the groups in the contralateral striatum (not shown), so stereological quantification was only performed in the ipsilateral striatum. Overexpression of α-syn led to the appearance of numerous MHC II+ microglia in the ipsilateral striatum at 4 weeks, and this remained elevated after 8 weeks in the control group (Fig. 6D). At 4 weeks, DFO treated and ctr animals showed similar numbers of MHC II+ cells (Fig. 6D), although this was highly variable within the DFO group. However, the number of MHC II+ cells in the DFO animals showed a trend toward a decrease at 8 weeks when compared to DFO animals at 4 weeks ($F_{1,13} = 3.9$ $p = 0.07$) or to the control group at 8 weeks ($F_{1,15} = 3.6$ $p = 0.07$) (Figs. 6B&D).

We noticed that the MHC II+ cells were preferentially present in the dorso-lateral striatum (Fig. 6C). Interestingly, numerous MHC II+ cells were located in the corpus callosum (not shown) and at the border with the striatum (Fig. 6C white arrow) in all animals at all time points. It is not clear at this moment whether the microglia in the striatum were resident cells that increased their MHC II expression or migrating cells traveling along the white matter of the corpus callosum. Inspection of phagocytic activity (CD68) did not result in any significant differences across the groups at the level of striatum; at all time points CD68 expression was low or absent.

Iron chelation did not prevent the infiltration of CD4 + cells

We investigated the effect iron chelation had on the adaptive immune response by quantifying helper T cell infiltration. Based on previous research of others and ourselves, we focused specifically on the CD4 population, which is suggested to be the most relevant to the neurodegenerative process (Brochard et al., 2009; Reynolds et al., 2010). The presence of CD4+ cells in the uninjected SN was rare in both groups at all time points (Table 2). α-Syn overexpression led to a strong early infiltration of CD4 T cells into the injected SN; this response was decreased by 8 weeks, at which point few CD4 T cells were still present in the parenchyma of the SN (Table 2). This pattern was similar in the DFO group, but the early infiltration was of slightly lower magnitude than that in the ctr group (Table 2).

The same magnitude of cytotoxic T cell (CD8+) infiltration was induced at 4 weeks by α-syn overexpression in both the DFO (44.2 ± 20.5) and ctr (55.5 ± 16.7) groups, and this expression decreased with time (11.6 ± 2.8 DFO and 11.5 ± 3.4 ctr). No helper

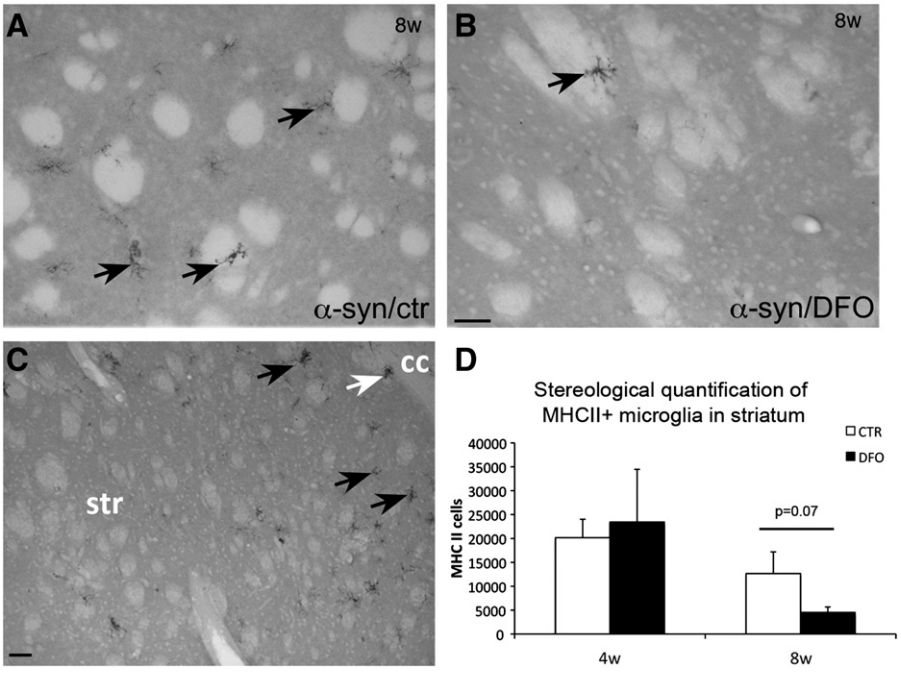

Fig. 6. Photomicrograph illustrating the MHC II+ cells in the ipsilateral side of the striatum 8 weeks post-transduction. Photos show striatal sections immunostained for MHC II from animals overexpressing α-syn and treated with ctr (A) or DFO (B) at 8 weeks post-surgery. Numerous MHC II+ cells (black arrows) were found in the α-syn/ctr group (A), whereas they were more scarcely observed in the α-syn/ctr group (B). (C) Photo shows a representative example of the lateralized presence of MHC II+ cells (black arrows) in the striatum; on occasion, cells in and at the border with the corpus callosum were observed (white arrow). (G) Bar graph illustrating the stereological quantification of MHCII+ microglia in the striatum (cell number ± SEM). DFO animals showed a trend toward fewer MHCII+ cells at 8 weeks when compared to the DFO group at 4 weeks ($F_{1,13} = 3.9$ $p = 0.07$) or to the control group at 8 weeks ($F_{1,15} = 3.6$ $p = 0.07$). The scale bar in B is 50 μm and applies to A; the scale bar in C is 100 μm. α-syn, alpha-synuclein, ctr, control; DFO, deferoxamine; cc: corpus callosum; str: striatum.

Table 2
Total number of infiltrated CD4+ T cells in substantia nigra.

Group	Time	Contralateral	Ipsilateral
α-syn/ctr	4 weeks	6.0 ± 1.6	1148.3 ± 269.9
	8 weeks	7.4 ± 2.1	124.2 ± 32.2**
α-syn/DFO	4 weeks	10.0 ± 2.9	839.8 ± 222.4
	8 weeks	9.7 ± 3.7	94.8 ± 32.9**

Number of CD4+ cells throughout the SN of animals treated with DFO (α-syn/DFO) or with vehicle (α-syn/ctr). An observer blind to the samples' identities counted the total number of cells in a series of representative sections as explained in the Materials and methods section. Numbers are group means ± SEM. Statistical analysis: one way ANOVA **$p < 0.01$ compared to the same group at earlier time point.

or cytotoxic T cell infiltration was observed in the striatum in any group at any time point.

MHC II expression correlated with α-syn aggregation

When we cross-analyzed several of the parameters studied, we found that the number of large striatal α-syn+ aggregates (>10 μm^2) in the ctr animals showed a strong correlation with the number of MHC II+ microglia in the striatum at 8 weeks (RSquare = 0.86 p = 0.0003). This finding suggests that α-syn overexpression leads to the presence of α-syn species that are handled in such a way as to be cleaved and loaded into the MHC II complex; this, in turn, results in MHC II accumulation in the membranes of the microglia (*i.e.*, enhanced expression). This correlation was, however, absent in the DFO animals.

We also observed that the number of CD4+ cells in SN was strongly positively correlated with MHC II scores at 4 weeks in the ctr group (RSquare = 0.79, p = 0.01), and this correlation disappeared at 8 weeks. In the DFO group, this correlation was moderate at 4 weeks but became significant at 8 weeks (RSquare 0.62, p = 0.03), pointing to a different and persistent immune response that correlated with a slower progression of the neurodegenerative process. Moreover, at 8 weeks, the number of CD4 cells in the SN showed a strong correlation with the MHC II microglia in the striatum of DFO animals (RSquare = 0.76, p = 0.009), pointing towards an immune response orchestrated from the SN that targets distant axons in the striatum.

Iron chelation attenuated one of the motor defects induced by α-syn overexpression

The unilateral overexpression of the transgene allowed us to explore the presence of motor abnormalities in these animals by addressing bias in the use of the paws through two different approaches: drug free tests (stepping and cylinder tests) and amphetamine-induced rotations (see Material and methods section). We addressed the use of the contralateral forepaw by the so-called stepping test, which was performed at 8 weeks (Fig. 7B). In general, naïve rats tend to perform fewer steps in the forward direction than the backward direction (approximately 15-20% less), and this number is greatly affected by dopaminergic lesions. Indeed α-syn overexpression in the ctr animals led to a decrease in the number of adjusting steps in the forward direction compared to the backward direction (-44%) (Fig. 7B). However, DFO treatment prevented this decrease, and the number of adjusting steps was only 17% lower than the number of backward steps, similar to what is observed in naïve animals.

The cylinder test, another measure of the paw use, was performed at both 4 and 8 weeks post-surgery (Fig. 7A). The ctr rats showed a significant decrease in the use of the ipsilateral paw after 8 weeks after transduction compared to the early time point. The DFO treatment did not prevent this decrease, and DFO rats also used the ipsilateral paw less at 8 weeks than at 4 weeks (Fig. 7A).

To further determinate changes in the behavior and to investigate the decrease of DA release/content in the striatum, amphetamine-induced rotations were monitored at 8 weeks, but no significant changes (bias in rotations) were observed in the groups; this finding was most likely due to the limited cell death observed in both α-syn groups (not shown).

Discussion

In vitro studies suggest that iron promotes α-syn aggregation; however, it is still debated whether iron has a role in the process initiated by α-syn mishandling that leads, ultimately, to cell death (Golts et al., 2002, 2004; Hashimoto et al., 1999). Here, we investigated the effect of chronic use of the iron chelator DFO in an α-syn rAAV vector-based model of PD. Unilateral overexpression of human α-syn in the ventral midbrain leads to progressive α-syn accumulation and dopaminergic cell death in rats. Chronic intranasal DFO did not prevent the loss of dopaminergic nigral neurons and striatal fibers; however, it improved motor performance, decreased the number and size of α-syn+ aggregates, and modified immune responses compared to the ctr group. Our results suggest that iron availability may modulate α-syn-induced pathology and/or the response to neurodegeneration in the brain by the adaptive immune system and result, ultimately, in better motor performance.

DFO was the first iron chelator approved for human use and is widely employed in studies of neurodegeneration (Brittenham et al., 1994). DFO can cross the blood brain barrier, although peripheral

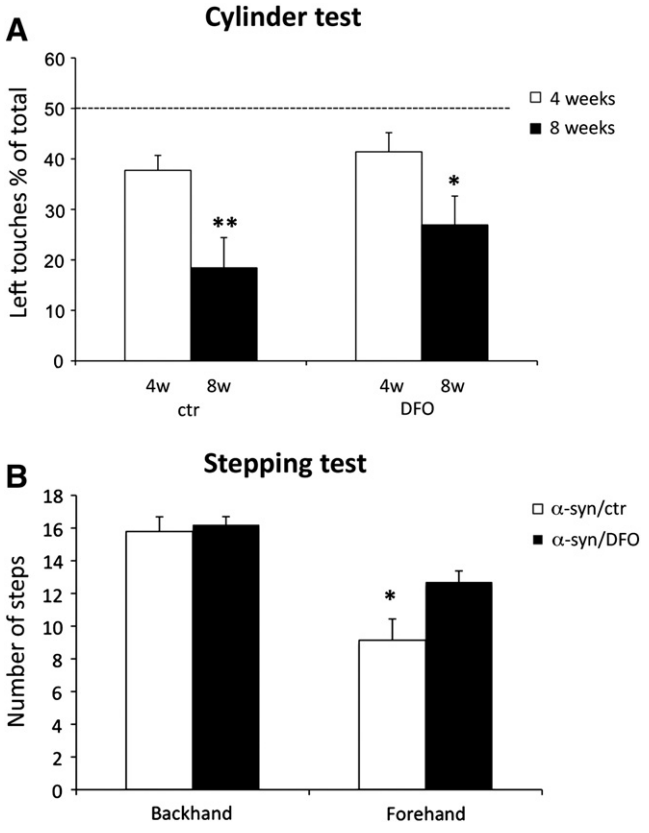

Fig. 7. Analysis of spontaneous motor behavior in animals overexpressing α-syn and treated with ctr or with DFO. Spontaneous limb use was evaluated with the cylinder test at 4 and 8 weeks post-surgery (A) Bars graph illustrating the average use of the left paw (as a % of the total ± SEM) per group at all time points. Both the α-syn/ctr and DFO groups showed a deficit in left paw use at 8 weeks when compared to the values obtained at 4 weeks. One-way ANOVA time effect (**) $p < 0.01$ and (*) $p < 0.05$ compared to the same group at the earlier time point. The stepping test was performed 8 weeks after surgery. (B) Bars represent the number of steps performed in the forward and backward directions (average ± SEM). Animals in the α-syn/DFO group performed significantly better in the backhand direction compared to the α-syn/ctr group; this parameter most strongly affected by dopaminergic neurotransmission failure; *$p < 0.05$ different from control group; One-way ANOVA ($F_{1,16} = 7.0$, $p = 0.01$). ANOVA, analysis of variance; α-syn, alpha-synuclein, ctr, control; DFO, deferoxamine.

administration can lead to undesired peripheral effects at dose sufficient to achieve effective CNS levels (Palmer et al., 1994). However, intranasal administration has been shown to diminish this problem by more efficiently targeting the brain *vs.* other peripheral tissues (Hanson et al., 2009). Hanson et al. showed that, 25 min after delivery, of 6 mg of DFO intranasally in rats, DFO levels are significantly higher levels in brain areas such as the midbrain and striatum (1.7 μM) compared to intravenous delivery of DFO (Hanson et al., 2009). In fact, chronic intranasal DFO has been shown to reduce pathological changes and improve behavioral defects in AD transgenic models (Fine et al., 2012; Guo et al., 2013a,b). Here, we applied this approach to a PD animal model. Analysis of the SN with Perls staining, a marker for iron (Fe^{3+}), showed that α-syn overexpression led to a time-dependent increase in cells containing Fe^{3+} that was diminished by chronic DFO administration, supporting the central effect of the drug.

Genetic or pharmacological iron chelation (intra-cerebral DFO or peripheral clioquinol or VK28) has previously resulted in neuroprotection in toxic PD models (Ben-Shachar et al., 1991; Kaur et al., 2003; Matarredona et al., 1997; Santiago et al., 2000; Shachar et al., 2004; Xu et al., 2008; Zhu et al., 2007). In contrast to our approach, these were mostly acute toxic models such as MPTP or 6-OHDA, and most of the laboratory administered the iron chelator before or simultaneously with the neurotoxin. McCormack et al., 2005 used chronic paraquat intoxication in genetically modified ferritin transgenic mice (shown to be more resistant to oxidative stress). We speculate that this approach is more efficient in terms of neuroprotection than the drug-treatment approach used here (McCormack et al., 2005). Together, these findings support the ability of pre-existing iron chelation to protect against oxidative stress-related insults, while our model is based on protein mishandling, and the DFO treatment was initiated 1 week after rAAV injection. Our design may be closer to the approach of Zhu et al., who used one intracerebral dose of the proteasome inhibitor lactacystin to induce progressive DAergic cell death over 28 days (Zhu et al., 2010). In their papers, both pharmacological and genetic iron chelation protected neurons and partially prevented the proteasomal inhibition and iron accumulation; although this effect was less efficiently if the pharmacological iron chelation was initiated after administration of the toxin. We speculate that the pharmacological iron chelation in our model may have led to a more efficient proteosomal degradation of the α-syn, as in Zhu et al., 2007, 2010, which could result in the positive outcomes we described. In our approach, chronic treatment did not protect dopaminergic neurons from α-syn-induced cell death as shown by the significant reduction of SN TH+ neurons (injected *vs.* uninjected side). Similarly, ipsilaterally decreased striatal dopaminergic innervation was observed despite DFO treatment, indicating that the iron chelation also failed to protect the fibers of α-syn expressing neurons. Notably, we only tested one dose of DFO; therefore, we cannot rule out the possibility that higher doses or the same dose administered prior to rAAV injection could produce more efficient cellular neuroprotection. However, iron increases do not precede, but rather follow, dopaminergic cell death in MPTP intoxicated monkeys, supporting a role for the metal in the progression of the neurodegeneration but not its onset (He et al., 2003). Therefore, we suggest that iron chelation cannot protect against the early α-syn-induced dopaminergic cell death but may contribute to delaying neurodegenerative progression.

Chronic DFO resulted in a decrease in the number α-syn+ formations, suggesting that iron chelation influences the ability of neurons to handle α-syn. *In vivo* α-syn increased toxicity has been associated with increases in the number of aggregates in some cases (Azeredo da Silveira et al., 2009; Chen and Feany, 2005), and this toxicity has been associated with a decrease in the number of aggregates in other cases (Gorbatyuk et al., 2008); however, normally, the quantification in these studies was performed on cell body inclusions and not striatal terminals as we have done. α-Syn+ formations increased in number and size with time, in agreement with our previous observations in the model (Decressac et al., 2011; Kirik et al., 2002; Sanchez-Guajardo et al., 2010); however, DFO treatment prevented the increase in the number of formations. These observations were also true when analyzing VMAT2+ pathological staining, confirming that these abnormal neurite formations also have VMAT2 accumulations as previously observed (Decressac et al., 2012). However, our data suggest that VMAT2 is incorporated later and that DFO prevents the early entrapment of VMAT2 in the aggregates; although DFO did not prevent posterior long-term incorporation into the existing aggregates. Similar to our results, a recent study reported reduced α-syn toxicity with concomitant decreases in pathological accumulations in the striatum (Oueslati et al., 2012). Iron chelation could influence not only the neuronal handling but also the nature of the accumulated α-syn. It is known that α-syn can directly bind to iron and other metals and lead to changes in conformation and/or solubility (for a review see (Wright and Brown, 2008)). Indeed *in vitro*, iron binds α-syn and promotes its aggregation by inducing α-syn oxidation (Cole et al., 2005; Golts et al., 2002; Gotz et al., 2004; Hashimoto et al., 1999). We speculate that, upon iron chelation, α-syn is less prone to aggregate and that the decrease of α-syn aggregation leads to the more efficient neuronal performance suggested by the superior performance in the stepping test. Chronic DFO significantly prevented the α-syn-induced inability of the contralateral forepaw to initiate movements, but no improvement was observed in the cylinder test; this finding most likely indicates that these tests address different basal ganglia functions. The improved performance of the DFO animals at 8 weeks occurred despite the loss of TH+ fibers in the striatum, suggesting that decreased iron availability may protect the remaining fibers and result in more efficient neurotransmission compared to the ctr animals. Indeed, it has been recently shown that, in the rAAV α-syn PD model, there is a progressive decrease in DA neurotransmission efficiency and reuptake that precedes fiber loss, which is, therefore, related to the presence of pathological α-syn in the presynaptic neuron (Lundblad et al., 2012). Also in the α-syn rAAV model, reduction in DA release correlates with a decrease in vesicles that is associated with pathological α-syn+ accumulations (Gaugler et al., 2012). This finding may also be related to the lower number of VMAT2 aggregates we observed that would affect DA homeostasis in the terminals differently and therefore affect neuronal transmission.

At this point, we cannot rule out the possibility that iron chelators could, initially or in parallel, act on the microglia to induce a response that may determine how neurons handle α-syn. Indeed, ferritin and iron levels have been previously related to microglia activation (Kaneko et al., 1989; Mehlhase et al., 2006). Microglia activation induces a decrease in ferritin levels that, in turn, contributes to the oxidative stress (Mehlhase et al., 2006) that may participate in the neuronal death in PD (Tanaka et al., 1994). The absence of iron decreases the levels of pro-inflammatory cytokines released by macrophages such as TNFα, IL-1 and IL-6 (Serafin-Lopez et al., 2004; Siglienti et al., 2006; Zhang et al., 2011). Therefore, the chelation of iron by DFO could modulate microglia activation, which, in turn, may exert the neuroprotective effect that led to the observed changes in the PD model herein. Accordingly, it has been shown that attenuation of microglia with minocycline, a drug shown that has also been shown to be an iron chelator, can prevent MPTP toxicity (Grenier et al., 2000; Wu et al., 2002).

We have previously shown that MHC II expression correlates with the availability of neurons and fibers expressing α-syn (Sanchez-Guajardo et al., 2010). Moreover, microglia expression of the human homologue of MHC II correlates with α-syn deposition in the brains of PD patients (McGeer et al., 1988). Here, we again show a correlation of MHC II expression with the presence of α-syn aggregates in the striatum. This correlation was absent in the DFO animals, which suggests a difference in the α-syn species generated and therefore, a different α-syn-induced microglia response to iron chelation. We believe that, among other factors, the type of α-syn generated by the neurons determines the type of

immune outcome elicited by the microglia. Alternatively, the mechanisms used by dopaminergic neurons to handle α-syn upon iron chelation may account for the reduced α-syn+ accumulations and the parallel decrease in the number of MHC II+ microglia in the striatum, as there may be less available α-syn to load into the MHC II complexes. Whatever the reason for the decrease in MHC II expression by microglia, this decrease may be the reason behind the different correlations between CD4+ cell infiltration and MHC II expression because CD4+ cell survival/activation is dependent on the interactions of microglia with MHC II. Indeed, a correlation between CD4 and MHC II expression in the SN was found earlier in the control animals than in the DFO, supporting a differential modulation of the neuroinflammatory response.

In conclusion, we show here that, although intranasal delivery of 6 mg DFO (3 times/week) failed to protect against the initial α-syn-induced dopaminergic cell loss, it led to changes in the number and nature of α-syn accumulations in fibers and the deposition of VMAT in these aggregates, which correlated with a trend toward downregulation of MHC II+ microglia in the striatum and a partial amelioration of deficits in motor performance. Taken together, our findings suggest that iron may modulate the handling of α-syn in the CNS, and our findings support the potential therapeutic use of intranasally administration DFO for PD.

Supplementary data to this article can be found online at http://dx.doi.org/10.1016/j.expneurol.2013.03.017.

Acknowledgments

The authors acknowledge financial support from the Lundbeck Foundation, the Danish Research Council and the Danish Parkinson Foundation (to MRR). VSG is a postdoctoral fellow from the Lundbeck Foundation. The authors wish to thank Gitte Toft for excellent technical assistance.

References

Azeredo da Silveira, S., Schneider, B.L., Cifuentes-Diaz, C., Sage, D., Abbas-Terki, T., Iwatsubo, T., Unser, M., Aebischer, P., 2009. Phosphorylation does not prompt, nor prevent, the formation of alpha-synuclein toxic species in a rat model of Parkinson's disease. Hum. Mol. Genet. 18, 872–887.

Beal, M.F., 1992. Does impairment of energy metabolism result in excitotoxic neuronal death in neurodegenerative illnesses? Ann. Neurol. 31, 119–130.

Ben-Shachar, D., Eshel, G., Finberg, J.P., Youdim, M.B., 1991. The iron chelator desferrioxamine (Desferal) retards 6-hydroxydopamine-induced degeneration of nigrostriatal dopamine neurons. J. Neurochem. 56, 1441–1444.

Ben-Shachar, D., Eshel, G., Riederer, P., Youdim, M.B., 1992. Role of iron and iron chelation in dopaminergic-induced neurodegeneration: implication for Parkinson's disease. Ann. Neurol. 32, S105–S110 (Suppl.).

Berg, D., Gerlach, M., Youdim, M.B., Double, K.L., Zecca, L., Riederer, P., Becker, G., 2001. Brain iron pathways and their relevance to Parkinson's disease. J. Neurochem. 79, 225–236.

Borie, C., Gasparini, F., Verpillat, P., Bonnet, A.M., Agid, Y., Hetet, G., Brice, A., Durr, A., Grandchamp, B., 2002. Association study between iron-related genes polymorphisms and Parkinson's disease. J. Neurol. 249, 801–804.

Brittenham, G.M., Griffith, P.M., Nienhuis, A.W., McLaren, C.E., Young, N.S., Tucker, E.E., Allen, C.J., Farrell, D.E., Harris, J.W., 1994. Efficacy of deferoxamine in preventing complications of iron overload in patients with thalassemia major. N. Engl. J. Med. 331, 567–573.

Brochard, V., Combadiere, B., Prigent, A., Laouar, Y., Perrin, A., Beray-Berthat, V., Bonduelle, O., Alvarez-Fischer, D., Callebert, J., Launay, J.M., Duyckaerts, C., Flavell, R.A., Hirsch, E.C., Hunot, S., 2009. Infiltration of CD4+ lymphocytes into the brain contributes to neurodegeneration in a mouse model of Parkinson disease. J. Clin. Invest. 119, 182–192.

Burger, C., Gorbatyuk, O.S., Velardo, M.J., Peden, C.S., Williams, P., Zolotukhin, S., Reier, P.J., Mandel, R.J., Muzyczka, N., 2004. Recombinant AAV viral vectors pseudotyped with viral capsids from serotypes 1, 2, and 5 display differential efficiency and cell tropism after delivery to different regions of the central nervous system. Mol. Ther. 10, 302–317.

Castellani, R.J., Siedlak, S.L., Perry, G., Smith, M.A., 2000. Sequestration of iron by Lewy bodies in Parkinson's disease. Acta Neuropathol. 100, 111–114.

Chen, L., Feany, M.B., 2005. Alpha-synuclein phosphorylation controls neurotoxicity and inclusion formation in a Drosophila model of Parkinson disease. Nat. Neurosci. 8, 657–663.

Cole, N.B., Murphy, D.D., Lebowitz, J., Di Noto, L., Levine, R.L., Nussbaum, R.L., 2005. Metal-catalyzed oxidation of alpha-synuclein: helping to define the relationship between oligomers, protofibrils, and filaments. J. Biol. Chem. 280, 9678–9690.

Conway, K.A., Harper, J.D., Lansbury Jr., P.T., 2000. Fibrils formed *in vitro* from alpha-synuclein and two mutant forms linked to Parkinson's disease are typical amyloid. Biochemistry 39, 2552–2563.

Cullen, V., Lindfors, M., Ng, J., Paetau, A., Swinton, E., Kolodziej, P., Boston, H., Saftig, P., Woulfe, J., Feany, M.B., Myllykangas, L., Schlossmacher, M.G., Tyynela, J., 2009. Cathepsin D expression level affects alpha-synuclein processing, aggregation, and toxicity *in vivo*. Mol. Brain 2, 5.

Davies, P., Moualla, D., Brown, D.R., 2011. Alpha-synuclein is a cellular ferrireductase. PLoS One 6, e15814.

Decressac, M., Ulusoy, A., Mattsson, B., Georgievska, B., Romero-Ramos, M., Kirik, D., Bjorklund, A., 2011. GDNF fails to exert neuroprotection in a rat alpha-synuclein model of Parkinson's disease. Brain 134, 2302–2311.

Decressac, M., Mattsson, B., Bjorklund, A., 2012. Comparison of the behavioural and histological characteristics of the 6-OHDA and alpha-synuclein rat models of Parkinson's disease. Exp. Neurol. 235, 306–315.

Double, K.L., Gerlach, M., Youdim, M.B., Riederer, P., 2000. Impaired iron homeostasis in Parkinson's disease. J. Neural. Transm. Suppl. 37–58.

Ebeling, W., Hennrich, N., Klockow, M., Metz, H., Orth, H.D., Lang, H., 1974. Proteinase K from Tritirachium album Limber. Eur. J. Biochem. 47, 91–97.

Febbraro, F., Giorgi, M., Caldarola, S., Loreni, F., Romero-Ramos, M., 2012. alpha-Synuclein expression is modulated at the translational level by iron. NeuroReport 23, 576–580.

Fine, J.M., Baillargeon, A.M., Renner, D.B., Hoerster, N.S., Tokarev, J., Colton, S., Pelleg, A., Andrews, A., Sparley, K.A., Krogh, K.M., Frey, W.H., Hanson, L.R., 2012. Intranasal deferoxamine improves performance in radial arm water maze, stabilizes HIF-1alpha, and phosphorylates GSK3beta in P301L tau transgenic mice. Exp. Brain Res. 219, 381–390.

Friedlich, A.L., Tanzi, R.E., Rogers, J.T., 2007. The 5′-untranslated region of Parkinson's disease alpha-synuclein messenger RNA contains a predicted iron responsive element. Mol. Psychiatry 12, 222–223.

Gaugler, M.N., Genc, O., Bobela, W., Mohanna, S., Ardah, M.T., El-Agnaf, O.M., Cantoni, M., Bensadoun, J.C., Schneggenburger, R., Knott, G.W., Aebischer, P., Schneider, B.L., 2012. Nigrostriatal overabundance of alpha-synuclein leads to decreased vesicle density and deficits in dopamine release that correlate with reduced motor activity. Acta Neuropathol. 123, 653–669.

Georgievska, B., Kirik, D., Bjorklund, A., 2004. Overexpression of glial cell line-derived neurotrophic factor using a lentiviral vector induces time- and dose-dependent downregulation of tyrosine hydroxylase in the intact nigrostriatal dopamine system. J. Neurosci. 24, 6437–6445.

Gerlach, M., Ben-Shachar, D., Riederer, P., Youdim, M.B., 1994. Altered brain metabolism of iron as a cause of neurodegenerative diseases? J. Neurochem. 63, 793–807.

Giasson, B.I., Murray, I.V., Trojanowski, J.Q., Lee, V.M., 2001. A hydrophobic stretch of 12 amino acid residues in the middle of alpha-synuclein is essential for filament assembly. J. Biol. Chem. 276, 2380–2386.

Golts, N., Snyder, H., Frasier, M., Theisler, C., Choi, P., Wolozin, B., 2002. Magnesium inhibits spontaneous and iron-induced aggregation of alpha-synuclein. J. Biol. Chem. 277, 16116–16123.

Gorbatyuk, O.S., Li, S., Sullivan, L.F., Chen, W., Kondrikova, G., Manfredsson, F.P., Mandel, R.J., Muzyczka, N., 2008. The phosphorylation state of Ser-129 in human alpha-synuclein determines neurodegeneration in a rat model of Parkinson disease. Proc. Natl. Acad. Sci. U. S. A. 105, 763–768.

Gotz, M.E., Double, K., Gerlach, M., Youdim, M.B., Riederer, P., 2004. The relevance of iron in the pathogenesis of Parkinson's disease. Ann. N. Y. Acad. Sci. 1012, 193–208.

Grenier, D., Huot, M.P., Mayrand, D., 2000. Iron-chelating activity of tetracyclines and its impact on the susceptibility of *Actinobacillus actinomycetemcomitans* to these antibiotics. Antimicrob. Agents Chemother. 44, 763–766.

Gundersen, H.J., Jensen, E.B., 1987. The efficiency of systematic sampling in stereology and its prediction. J. Microsc. 147 (Pt 3), 229–263.

Guo, C., Wang, P., Zhong, M.L., Wang, T., Huang, X.S., Li, J.Y., Wang, Z.Y., 2013a. Deferoxamine inhibits iron induced hippocampal tau phosphorylation in the Alzheimer transgenic mouse brain. Neurochem. Int. 62, 165–172.

Guo, C., Wang, T., Zheng, W., Shan, Z.Y., Teng, W.P., Wang, Z.Y., 2013b. Intranasal deferoxamine reverses iron-induced memory deficits and inhibits amyloidogenic APP processing in a transgenic mouse model of Alzheimer's disease. Neurobiol Aging 34, 562–575.

Gutteridge, J.M., 1992. Ageing and free radicals. Med. Lab. Sci. 49, 313–318.

Hanson, L.R., Roeytenberg, A., Martinez, P.M., Coppes, V.G., Sweet, D.C., Rao, R.J., Marti, D.L., Hoekman, J.D., Matthews, R.B., Frey II, W.H., Panter, S.S., 2009. Intranasal deferoxamine provides increased brain exposure and significant protection in rat ischemic stroke. J. Pharmacol. Exp. Ther. 330, 679–686.

Hashimoto, M., Hsu, L.J., Xia, Y., Takeda, A., Sisk, A., Sundsmo, M., Masliah, E., 1999. Oxidative stress induces amyloid-like aggregate formation of NACP/alpha-synuclein *in vitro*. NeuroReport 10, 717–721.

He, Y., Thong, P.S., Lee, T., Leong, S.K., Mao, B.Y., Dong, F., Watt, F., 2003. Dopaminergic cell death precedes iron elevation in MPTP-injected monkeys. Free Radic. Biol. Med. 35, 540–547.

Hoepken, H.H., Korten, T., Robinson, S.R., Dringen, R., 2004. Iron accumulation, iron-mediated toxicity and altered levels of ferritin and transferrin receptor in cultured astrocytes during incubation with ferric ammonium citrate. J. Neurochem. 88, 1194–1202.

Kaneko, Y., Kitamoto, T., Tateishi, J., Yamaguchi, K., 1989. Ferritin immunohistochemistry as a marker for microglia. Acta Neuropathol. 79, 129–136.

Kaur, D., Yantiri, F., Rajagopalan, S., Kumar, J., Mo, J.Q., Boonplueang, R., Viswanath, V., Jacobs, R., Yang, L., Beal, M.F., DiMonte, D., Volitaskis, I., Ellerby, L., Cherny, R.A., Bush, A.I., Andersen, J.K., 2003. Genetic or pharmacological iron chelation prevents

MPTP-induced neurotoxicity *in vivo*: a novel therapy for Parkinson's disease. Neuron 37, 899–909.
Kirik, D., Rosenblad, C., Bjorklund, A., 1998. Characterization of behavioral and neurodegenerative changes following partial lesions of the nigrostriatal dopamine system induced by intrastriatal 6-hydroxydopamine in the rat. Exp. Neurol. 152, 259–277.
Kirik, D., Rosenblad, C., Burger, C., Lundberg, C., Johansen, T.E., Muzyczka, N., Mandel, R.J., Bjorklund, A., 2002. Parkinson-like neurodegeneration induced by targeted overexpression of alpha-synuclein in the nigrostriatal system. J. Neurosci. 22, 2780–2791.
Lundblad, M., Decressac, M., Mattsson, B., Bjorklund, A., 2012. Impaired neurotransmission caused by overexpression of alpha-synuclein in nigral dopamine neurons. Proc. Natl. Acad. Sci. U. S. A. 109 (9), 3213–3219.
Marti, M.J., Tolosa, E., Campdelacreu, J., 2003. Clinical overview of the synucleinopathies. Mov. Disord. 18 (Suppl. 6), S21–S27.
Martin, W.R., Wieler, M., Gee, M., 2008. Midbrain iron content in early Parkinson disease: a potential biomarker of disease status. Neurology 70, 1411–1417.
Matarredona, E.R., Santiago, M., Cano, J., Machado, A., 1997. Involvement of iron in MPP+ toxicity in substantia nigra: protection by desferrioxamine. Brain Res. 773, 76–81.
McCormack, A.L., Atienza, J.G., Johnston, L.C., Andersen, J.K., Vu, S., Di Monte, D.A., 2005. Role of oxidative stress in paraquat-induced dopaminergic cell degeneration. J. Neurochem. 93, 1030–1037.
McGeer, P.L., Itagaki, S., Boyes, B.E., McGeer, E.G., 1988. Reactive microglia are positive for HLA-DR in the substantia nigra of Parkinson's and Alzheimer's disease brains. Neurology 38, 1285–1291.
Mehlhase, J., Gieche, J., Widmer, R., Grune, T., 2006. Ferritin levels in microglia depend upon activation: modulation by reactive oxygen species. Biochim. Biophys. Acta 1763, 854–859.
Miake, H., Mizusawa, H., Iwatsubo, T., Hasegawa, M., 2002. Biochemical characterization of the core structure of alpha-synuclein filaments. J. Biol. Chem. 277, 19213–19219.
Oakley, A.E., Collingwood, J.F., Dobson, J., Love, G., Perrott, H.R., Edwardson, J.A., Elstner, M., Morris, C.M., 2007. Individual dopaminergic neurons show raised iron levels in Parkinson disease. Neurology 68, 1820–1825.
Olsson, M., Nikkhah, G., Bentlage, C., Bjorklund, A., 1995. Forelimb akinesia in the rat Parkinson model: differential effects of dopamine agonists and nigral transplants as assessed by a new stepping test. J. Neurosci. 15, 3863–3875.
Oueslati, A., Paleologou, K.E., Schneider, B.L., Aebischer, P., Lashuel, H.A., 2012. Mimicking phosphorylation at serine 87 inhibits the aggregation of human alpha-synuclein and protects against its toxicity in a rat model of Parkinson's disease. J. Neurosci. 32, 1536–1544.
Palmer, C., Roberts, R.L., Bero, C., 1994. Deferoxamine posttreatment reduces ischemic brain injury in neonatal rats. Stroke 25, 1039–1045.
Paxinos, G., Watson, C., 2007. The Rat Brain in Stereotaxic Coordinates. Academic Press, London.
Perry, T.L., Yong, V.W., 1986. Idiopathic Parkinson's disease, progressive supranuclear palsy and glutathione metabolism in the substantia nigra of patients. Neurosci. Lett. 67, 269–274.
Reynolds, A.D., Stone, D.K., Hutter, J.A., Benner, E.J., Mosley, R.L., Gendelman, H.E., 2010. Regulatory T cells attenuate Th17 cell-mediated nigrostriatal dopaminergic neurodegeneration in a model of Parkinson's disease. J. Immunol. 184 (5), 2261–2271.
Ross, O.A., Braithwaite, A.T., Skipper, L.M., Kachergus, J., Hulihan, M.M., Middleton, F.A., Nishioka, K., Fuchs, J., Gasser, T., Maraganore, D.M., Adler, C.H., Larvor, L., Chartier-Harlin, M.C., Nilsson, C., Langston, J.W., Gwinn, K., Hattori, N., Farrer, M.J., 2008. Genomic investigation of alpha-synuclein multiplication and parkinsonism. Ann. Neurol. 63, 743–750.
Sanchez-Guajardo, V., Febbraro, F., Kirik, D., Romero-Ramos, M., 2010. Microglia acquire distinct activation profiles depending on the degree of alpha-synuclein neuropathology in a rAAV based model of Parkinson's disease. PLoS One 5, e8784.
Santiago, M., Matarredona, E.R., Granero, L., Cano, J., Machado, A., 2000. Neurotoxic relationship between dopamine and iron in the striatal dopaminergic nerve terminals. Brain Res. 858, 26–32.
Schallert, T., Fleming, S.M., Leasure, J.L., Tillerson, J.L., Bland, S.T., 2000. CNS plasticity and assessment of forelimb sensorimotor outcome in unilateral rat models of stroke, cortical ablation, parkinsonism and spinal cord injury. Neuropharmacology 39, 777–787.
Serafin-Lopez, J., Chacon-Salinas, R., Munoz-Cruz, S., Enciso-Moreno, J.A., Estrada-Parra, S.A., Estrada-Garcia, I., 2004. The effect of iron on the expression of cytokines in macrophages infected with Mycobacterium tuberculosis. Scand. J. Immunol. 60, 329–337.
Shachar, D.B., Kahana, N., Kampel, V., Warshawsky, A., Youdim, M.B., 2004. Neuroprotection by a novel brain permeable iron chelator, VK-28, against 6-hydroxydopamine lession in rats. Neuropharmacology 46, 254–263.
Siglienti, I., Bendszus, M., Kleinschnitz, C., Stoll, G., 2006. Cytokine profile of iron-laden macrophages: implications for cellular magnetic resonance imaging. J. Neuroimmunol. 173, 166–173.
Spillantini, M.G., Schmidt, M.L., Lee, V.M., Trojanowski, J.Q., Jakes, R., Goedert, M., 1997. Alpha-synuclein in Lewy bodies. Nature 388, 839–840.
Tanaka, M., Sotomatsu, A., Yoshida, T., Hirai, S., Nishida, A., 1994. Detection of superoxide production by activated microglia using a sensitive and specific chemiluminescence assay and microglia-mediated PC12h cell death. J. Neurochem. 63, 266–270.
Thomas, B., Beal, M.F., 2007. Hum. Mol. Genet. 16 (Spec No. 2:R183-194).
Thompson, K.J., Shoham, S., Connor, J.R., 2001. Iron and neurodegenerative disorders. Brain Res. Bull. 55, 155–164.
West, M.J., 1999. Stereological methods for estimating the total number of neurons and synapses: issues of precision and bias. Trends Neurosci. 22, 51–61.
Wright, J.A., Brown, D.R., 2008. Alpha-synuclein and its role in metal binding: relevance to Parkinson's disease. J. Neurosci. Res. 86, 496–503.
Wu, D.C., Jackson-Lewis, V., Vila, M., Tieu, K., Teismann, P., Vadseth, C., Choi, D.K., Ischiropoulos, H., Przedborski, S., 2002. Blockade of microglial activation is neuroprotective in the 1-methyl-4-phenyl-1,2,3,6-tetrahydropyridine mouse model of Parkinson disease. J. Neurosci. 22, 1763–1771.
Xu, L., Daly, T., Gao, C., Flotte, T.R., Song, S., Byrne, B.J., Sands, M.S., Parker Ponder, K., 2001. CMV-beta-actin promoter directs higher expression from an adeno-associated viral vector in the liver than the cytomegalovirus or elongation factor 1 alpha promoter and results in therapeutic levels of human factor X in mice. Hum. Gene Ther. 12, 563–573.
Xu, Q., Kanthasamy, A.G., Reddy, M.B., 2008. Neuroprotective effect of the natural iron chelator, phytic acid in a cell culture model of Parkinson's disease. Toxicology 245, 101–108.
Youdim, M.B., Ben-Shachar, D., Riederer, P., 1989. Is Parkinson's disease a progressive siderosis of substantia nigra resulting in iron and melanin induced neurodegeneration? Acta Neurol. Scand. Suppl. 126, 47–54.
Zecca, L., Youdim, M.B., Riederer, P., Connor, J.R., Crichton, R.R., 2004. Iron, brain ageing and neurodegenerative disorders. Nat. Rev. Neurosci. 5, 863–873.
Zhang, Z., Zhang, F., An, P., Guo, X., Shen, Y., Tao, Y., Wu, Q., Zhang, Y., Yu, Y., Ning, B., Nie, G., Knutson, M.D., Anderson, G.J., Wang, F., 2011. Ferroportin1 deficiency in mouse macrophages impairs iron homeostasis and inflammatory responses. Blood 118, 1912–1922.
Zhu, W., Xie, W., Pan, T., Xu, P., Fridkin, M., Zheng, H., Jankovic, J., Youdim, M.B., Le, W., 2007. Prevention and restoration of lactacystin-induced nigrostriatal dopamine neuron degeneration by novel brain-permeable iron chelators. FASEB J. 21, 3835–3844.
Zhu, W., Li, X., Xie, W., Luo, F., Kaur, D., Andersen, J.K., Jankovic, J., Le, W., 2010. Genetic iron chelation protects against proteasome inhibition-induced dopamine neuron degeneration. Neurobiol. Dis. 37, 307–313.
Zolotukhin, S., Byrne, B.J., Mason, E., Zolotukhin, I., Potter, M., Chesnut, K., Summerford, C., Samulski, R.J., Muzyczka, N., 1999. Recombinant adeno-associated virus purification using novel methods improves infectious titer and yield. Gene Ther. 6, 973–985.
Zolotukhin, S., Potter, M., Zolotukhin, I., Sakai, Y., Loiler, S., Fraites Jr., T.J., Chiodo, V.A., Phillipsberg, T., Muzyczka, N., Hauswirth, W.W., Flotte, T.R., Byrne, B.J., Snyder, R.O., 2002. Production and purification of serotype 1, 2, and 5 recombinant adeno-associated viral vectors. Methods 28, 158–167.